Studies of Dispersed Phase Size in a Helical Tube Reactor with a Liquid-liquid Heterogeneous System

[1, 2] Guang-Wen Chu, [1] Hai-Kui Zou, [1] Xiao Yu, [1] Yong Luo, [1] Jing Zhou, [1] Moses Arowo and [1, 2] Jian-Feng Chen
[1]*Research Center of the Ministry of Education for High Gravity Engineering and Technology, Beijing 100029, P.R. China.*
[2]*State Key Laboratory of Organic-Inorganic Composites, Beijing University of Chemical Technology, Beijing 100029, P.R. China.*
luoyong@mail.buct.edu.cn*

(Received on 13th August 2014, accepted in revised form 25th November 2014)

Summary: The size of the dispersed phase was a key variable of the liquid-liquid heterogeneous flow system. In this work, the Sauter mean diameter (SMD) of the dispersed phase in a novel helical tube reactor (HTR) was evaluated by using a castor oil-water system. Experimental results showed that the SMD decreased with the increased Reynolds number and volumetric flowrate ratio of water to oil. The SMD in the HTR with vertical charging was smaller ion between calculated and experimental data was within ±20% than that with parallel charging. A dimensionless correlation of SMD in the HTR was proposed and the deviation between calculated and experimental data was within ±20%.

Keywords: Helical tube reactor; Heterogeneous flow; Sauter mean diameter; Dispersed phase size; Correlation; charging component

Introduction

The curved tube was recognized as one of the process intensification devices for mixing, heat and mass transfer due to the generation of a secondary flow due to unbalanced centrifugal forces, enhanced cross-sectional mixing, reduction of the axial dispersion, and improved heat and mass transfer coefficient. An exhaustive review on the fundamentals including fluid mixing and flow phenomena, heat and mass transfer, and related models as well as the potential industrial applications of the curved tubes was published by Vashisth *et al.,* [1]. The ongoing research involved developing numerical methods to detail local variables, exploring new configurations such as tube-in-tube heat exchanger and further investigating on coiled flow inverter using as reactor, and flow characteristics of non-Newtonian liquid [2-9]. Liquid-liquid heterogeneous flow systems, e.g. two immiscible liquids are commonly encountered in oil, chemical and food industries. A key variable, the dispersed phase size, of the heterogeneous flow system has received comparatively little attention.

The size of the dispersed phase had a great influence on the effective interfacial area which benefited mass transfer and apparent reaction rate in a heterogeneous system [10]. The size of the dispersed phase was usually described by the ratio of the average volume to its surface area, i.e. Sauter mean diameter (SMD). The SMD links the surface area of the dispersed phase to its volume and hence to mass transfer and apparent reaction rate. It was thus extensively used in the studies of the effective interfacial area for liquid-liquid or gas-liquid systems [11].

Many methods have been developed to determine the size of dispersed phase. Physical methods have been employed, such as optical dual void probes techniques and photographic methods [10, 12-14]. In all of these physical methods, a local value of the dispersed phase size was determined. The installed probes however disturbed the flow, which resulted in deviations. Angeli and Hewitt found that the drop size distribution was strongly influenced by the pipe material under the same flow conditions, leading to a confined images analysis in practical applications [15]. Westerterp *et al.,* introduced a fast pseudo-first order reaction to evaluate the effective interfacial area of a gas-liquid system [16]. Chemical methods have been employed to measure the interfacial areas for liquid-liquid systems [17-20]. Whilst chemical reaction systems fulfilling the following: (1) the solubility of oil in the aqueous phase is very low, so mass transfer limitations in the oil phase can be neglected; (2) the reaction is sufficiently fast to consume all reagents in the film and no reagents will reach the bulk of the reaction phase; (3) no diffusion limitation of aqueous phase reagents occurs in the reaction zone: the concentration of reagents in the aqueous phase at the interface is approximately equal to the bulk

*To whom all correspondence should be addressed.

concentration. The mass transfer rate is thus a unique function of the physico-chemical properties of the system and independent of the hydrodynamic conditions.

The helical tube is one well-known type of curved tubes that has been used in a wide variety of applications, such as heat recovery processes, air conditioning and refrigeration systems, chemical reactors, and food and dairy processes. In present work, a novel helical tube reactor (HTR) consisted of a helical tube and charging component using as inlets of different reactants. The dispersed phase was pre-dispersed into the continuous phase in the charging component. Then the action of the secondary flow in the helical tube further decreased the size of the dispersed phase. A chemical method, as employed by Liang *et al.*,., was used to investigate the dispersed phase size in the HTR [19]. For the sake of observing the dispersing difference between a straight tube with the same diameter and effective length as the helical tube, comparative experiments were firstly carried out. The effects of Reynolds number (*Re*), volumetric flow ratio of water to oil (*R*), and charging position (*x*) on SMD were accessed. A dimensionless correlation of size of the dispersed phase (d_{VAM}) was finally proposed for the HTR with different type of charging component.

Experimental

Calculations

The principle of the measurement system is as following: when oil phase (castor oil containing 1mol/L acetic anhydride) and water phases mixed, acetic anhydride in the oil phase diffuses into the interface, and an irreversible hydrolysis reaction occurs

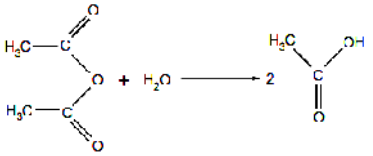

(1)

The reaction is sufficiently fast to consume all acetic anhydride in the film, so that the concentration in the bulk of the continuous phase equals zero. Water is defined as solution A and acetic anhydride as solution B. The interface reaction rate is written as:

$$-dC_B / d\tau = K_a a C_A C_B \qquad (2)$$

where C_A is approximately constant. The pseudo-first-order reaction rate constant can be assumed to be $K^{'} = K_a C_A$, and K' can be obtained based on the mass transfer theory. a and V_B are calculated by the following equations:

$$a = \pi d_{VAM}^2 \frac{N}{V_R} \qquad (3)$$

$$V_B = N \frac{\pi}{6} d_{VAM}^3 \qquad (4)$$

where $V_R = V_A + V_B$ and d_{VAM} was the Sauter mean diameter of the dispersed phase. The volume or volumetric flowrate ratio of phase A to B was defined as: $R = \frac{V_A}{V_B} = \frac{Q_A}{Q_B}$

Substituting Eq. (4) into Eq. (3) gave a as:

$$a = \frac{6}{d_{VAM}(R+1)} \qquad (5)$$

Substituting Eq. (5) into Eq. (2) gave:

$$-dC_B / d\tau = K^{'} C_B \frac{6}{d_{VAM}(R+1)} \qquad (6)$$

The mean reaction rate can be expressed as:

$$-dC_B / d\tau = \frac{C_{B0} - C_B}{\tau} \qquad (7)$$

Comparing Eq. (6) and Eq. (7), d_{VAM} can be written as:

$$d_{VAM} = 6K^{'}\tau \frac{C_B}{(C_{B0} - C_B)(R+1)} \qquad (8)$$

The mean residence time τ can be calculated by:

$$\tau = \frac{V_R}{Q_V} \qquad (9)$$

where $Q_V = Q_A + Q_B$. According to the mass balance of Eq. (2), the relationship between the concentration of acetic acid (C_C) in the water phase and the concentration of acetic anhydride (C_B) can be expressed as:

$$C_B = C_{B0} - \frac{1}{2} R C_C \qquad (10)$$

C_B can be determined by Eq. (10) if C_C in the water phase is known.

C_C in the water phase was measured by an automatic potentiometric titrimeter (ZDJ-2D, Beijing Xianqu Weifeng Technology Development Co., China) using NaOH solution.

$$C_C V_C = C_{NaOH} V_{NaOH} \qquad (11)$$

V_{NaOH} was the volume of NaOH solution consumed during titration. The concentration of NaOH solution was 0.0025 mol·L^{-1}, and the volume of the collected samples was 10 mL. Substituting Eq. (11) into Eq. (10), Eq. (10) reduces to:

$$C_B = C_{B0} - \frac{R V_{NaOH}}{800} \qquad (12)$$

Substituting Eq. (12) into Eq. (8), d_{VAM} can be calculated as:

$$d_{VAM} = \frac{6K'\tau(800C_{B0} - RV_{NaOH})}{R(R+1)V_{NaOH}} \qquad (13)$$

When V_{NaOH} was obtained by titration, d_{VAM} can be determined by Eq. (13).

Experiment setup

The experimental set-up is shown in Fig. 1. It consists of a helical tube, a charging component, two liquid storage tanks, a storage tank, two peristaltic pumps, a glass test-tube, and other accessories. The helical tube was connected to a charging component and oriented horizontally. The structural parameters of the helical tube are given in Table-1.

The schematic drawing of the charging components and *x*-coordinates for the charging positions are shown in Fig. 2. The inner diameter of the charging component for the continuous phase flow is 8 mm, and gradually decreases to 4mm in the charging section (see Fig. 2 (a)). According to the position of the outlet holes on the inner tube, charging component is divided into either a vertical type (V-type, two liquids with a vertical flow direction) or a parallel type (P-type, two liquids with a parallel flow direction). In the V-type charging component, the dispersed phase (oil) flows from the inner tube in a vertical direction to the continuous phase (water) through two 0.5 mm (diameter) jet orifices. In the P-type charging component, the dispersed phase (oil) flows from the inner tube in a parallel direction to the continuous phase (water) through a 1 mm (diameter) jet. The cross-sectional area in the charging section can be varied by moving the inner tube along the *x*-coordinate (see Fig. 2 (b) and (c)). The inner tube is welded on a flange. The position of the jet orifice in the inner tube along the *x*-coordinate can be changed by adjusting the number of gaskets on the right-hand side of the flange. The thickness of a gasket is 1 mm.

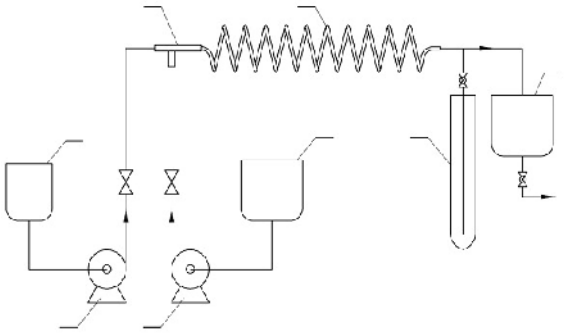

1-water tank, 2-water pump, 3-castor oil pump, 4-castor oil tank (containing acetic anhydride), 5-charging component, 6-helical tube, 7-storage tank, 8- glass test-tube for sample collection

Fig. 1: Experimental set-up.

Table-1: Structural parameters of helical tube

Inner diameter/mm	Bending diameter/mm	Pitch/mm	Number of circles
4	80	20	10

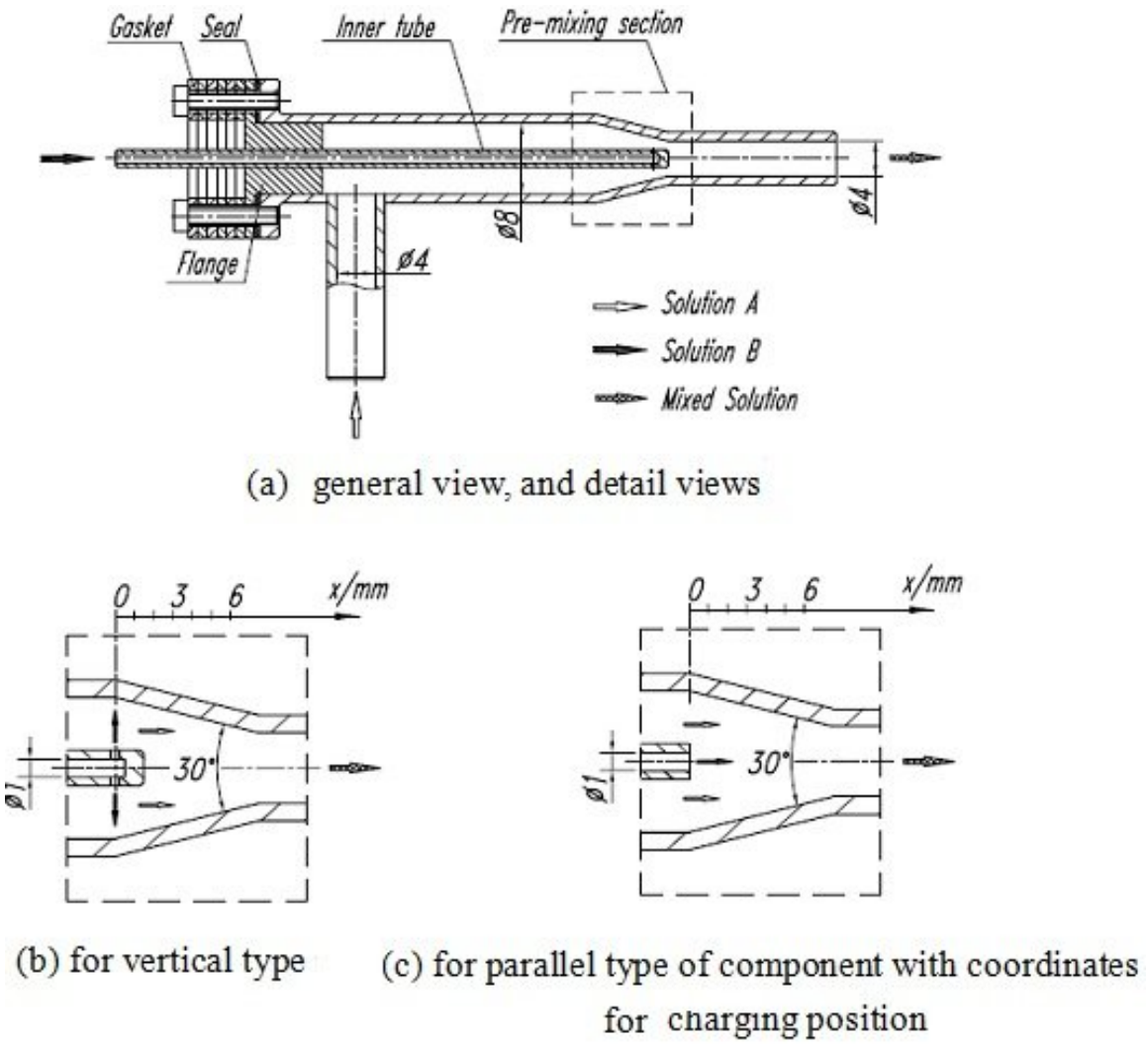

(a) general view, and detail views (b) for vertical type (c) for parallel type of component with coordinates for charging position

Fig. 2: Schematic drawing of charging components and *x* - coordinates for charging position.

Experimental Procedure

In this study, A was deionized water. Solution B was prepared by dissolving the required acetic anhydride in castor oil to obtain a homogeneous castor oil solution (containing 1 mol/L acetic anhydride). The physical properties of castor oil and acetic anhydride were given in Table-2.

Table-2: Physical properties of castor oil and acetic anhydride (20ºC).

Parameters	Castor oil	Acetic anhydride
Density (kg/m^3)	961	1082
Viscosity (Pa·s)	0.7	0.9×10^{-3}
Surface tension (N/m)	3.9×10^{-2}	3.55×10^{-2}

Solution B and A were stored in tank 4 and tank 1, respectively. Solution B and A were separately transported to the charging component by two peristaltic pumps. The oil phase from the jet orifices mixed primarily with the water phase in the charging component and then flowed into the helical tube. In the helical tube, both oil and water mixed continuously. The operation temperature was 20℃ at atmospheric pressure. A glass test-tube was set at the outlet of helical tube to collect the sample. The collected oil-water mixture separated quickly and 10 mL acetic acid solution was taken from the water layer by a syringe for analysis. The acetic acid concentrations of collected samples were titrated (see *calculations* section).

Results and discussion

Comparison of d_{VAM} in the helical tube and straight tube

The length of the straight tube and the helical tube is 1.9 m. Results of d_{VAM} in the helical tube and the straight tube are shown in Fig. 3, providing completely different values. The smallest d_{VAM} in the HTR was below 0.1 mm in a high *Re* region. Compared with the d_{VAM} in the straight tube, the d_{VAM} in the HTR decreased by 47.2~75% and 38.1~48.5% in low and high *Re* region, respectively. These results demonstrate that the secondary flow produced by the geometric configuration of the helical tube enhanced the radial mixing and dispersion of fluids.

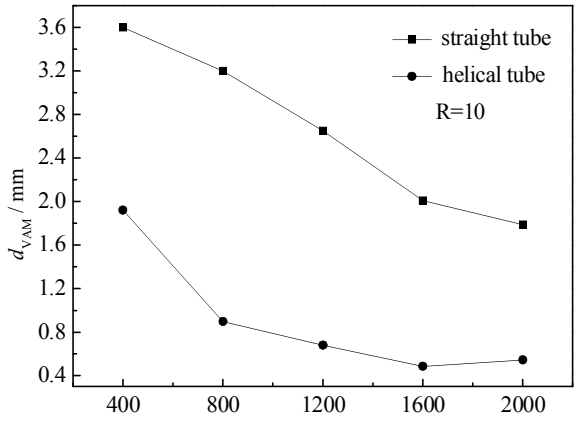

(a)

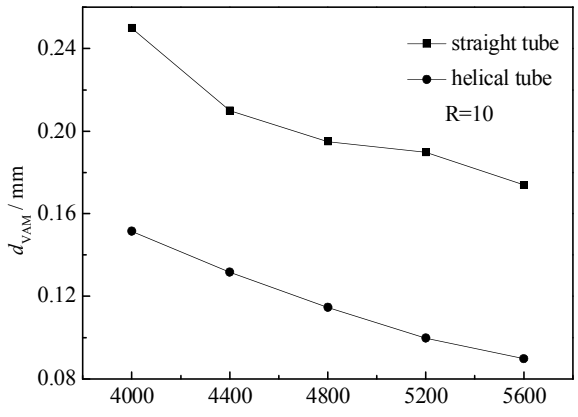

(b)

Fig. 3: Comparison of d_{VAM} in helical tube and straight tube. (a) in low *Re* region and (b) in high *Re* region

Effects of Re on d_{VAM}

For a certain geometric configuration of the helical tube, the *R*e of the continuous phase had a significant influence on the flow pattern and the intensity of the secondary flow in the helical tube. Increasing *R*e means the increase of energy input. High *R*e was favorable for breakup of the liquid into small droplets. Effects of *R*e on d_{VAM} in low *Re* region (400≤Re≤2000) and high *Re* region (4000≤Re≤5600) are shown in Fig. 4(a) and (b), respectively. It was shown that d_{VAM} decreased from 3.5 to 2.5 mm in the P-type charging component and from 3.5 to 0.75 mm in the V-type charging component in the low *R*e region. In the high *R*e region, d_{VAM} was smaller than 0.3 mm. The V-type charging component showed better pre-dispersion performance than the P-type charging component. Value of d_{VAM} can be reduced to below 0.1 mm in the HTR with V-type charging component when *R*e exceeds 5600.

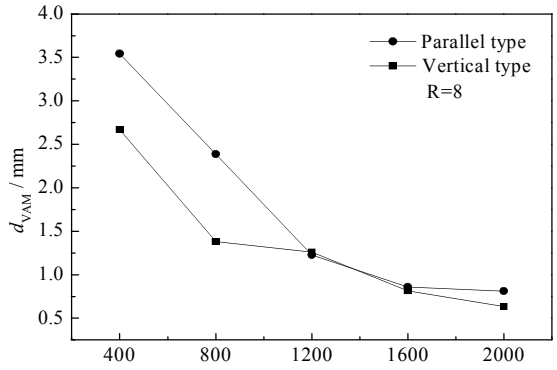

(a)

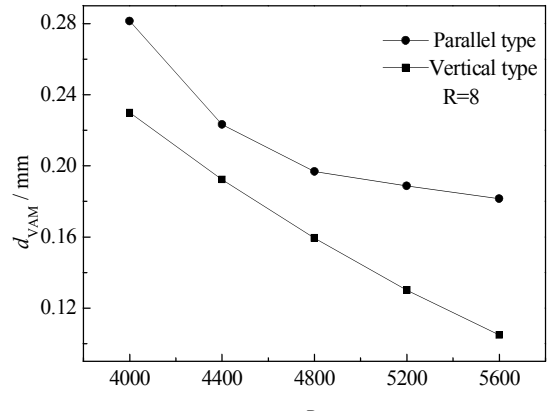

(b)

(a) in low *Re* region (400≤*Re*≤2000) and (b) in high *Re* region (4000≤*Re*≤5600)

Fig. 4: Effects of *Re* on d_{VAM} .

Effects of volumetric flowrate ratio on d_{VAM}

Volumetric flowrate ratio of water to oil was regulated by fixing water flowrate and varying oil flowrate. Effect of *R* from 8~12 on d_{VAM} is shown in Fig. 5 (a) and (b). d_{VAM} decreases with the increasing of *R*. The higher volumetric flowrate ratio meant less oil phase required to be dispersed under the same energy input, meaning a higher energy input per unit oil phase decreases d_{VAM}. There are large differences in d_{VAM} between the conditions of *R*=8 and *R*=10. The differences are small between the conditions of *R*=10 and *R*=12. In the high *Re* region, d_{VAM} decreased continuously and to below 0.1 mm as shown in Fig. 6 (a) and (b).

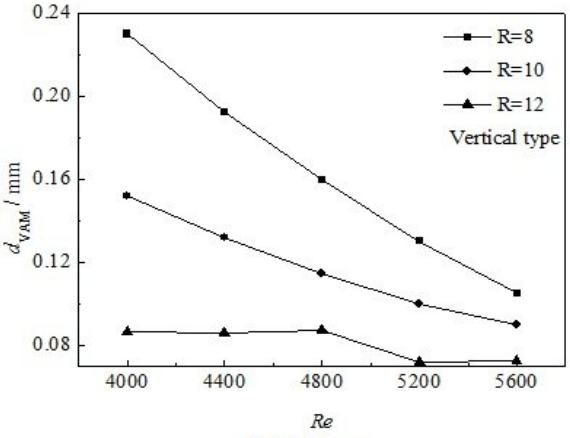

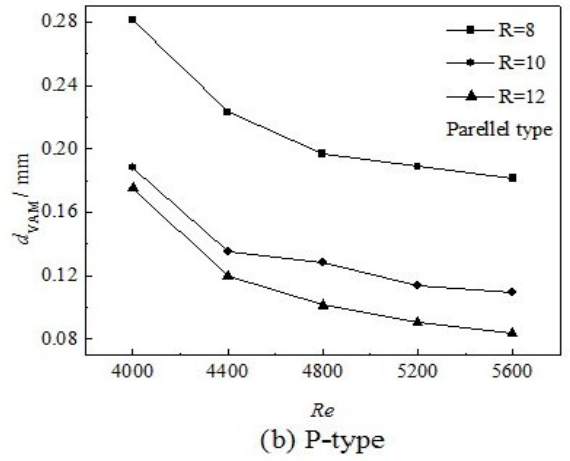

Fig. 5: Effects of volumetric flow ratio on d_{VAM} in low *Re* region, (a) V-type and (b) P-type

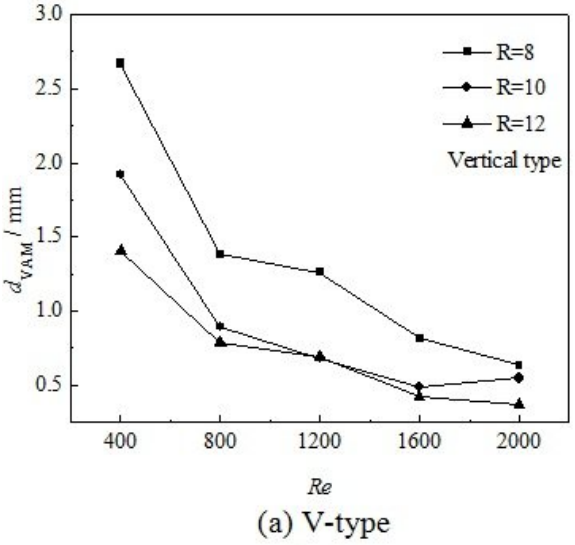

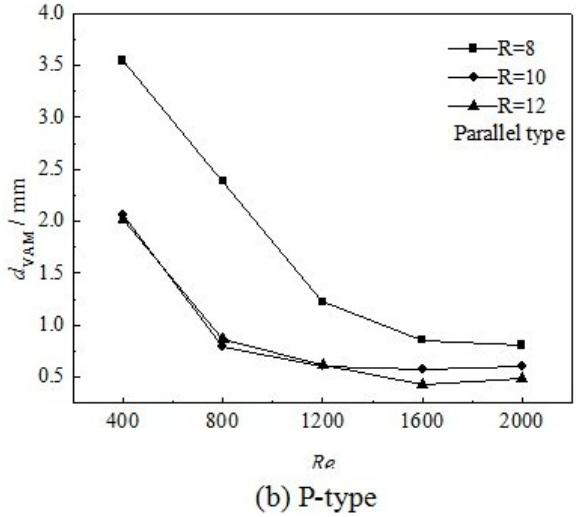

Fig. 6: Effects of volumetric flow ratio on d_{VAM} in high *Re* region, (a) V-type and (b) P-type.

Effect of charging position on d_{VAM}

As shown in Fig. 2, there are six charging positions in the charging section. The velocity of the continuous phase at each charging position is given in Table-3.

Table-3: Velocity of solution A at different charging positions.

x/mm	1	2	3	4	5	6
u/m·s^{-1} (*Re*=800)	0.07	0.09	0.1	0.12	0.16	0.2
u/m·s^{-1} (*Re*=4800)	0.45	0.53	0.61	0.75	0.9	1.2

When the oil phase is jetted from the inner tube in the charging section, the dispersion efficiency of the oil phase varied as a result of the different velocity of the continuous phase. With the increase of the velocity of the continuous phase, shear stress introduced by the continuous phase on the dispersed phase was strengthened. The size of the dispersed phase decreased due to a better peeling effect provided by the continuous phase. Hence a good dispersion effect was obtained. As shown in Fig. 7 (a) and (b), d_{VAM} decreased as the charging position changed from x = 1 to 6 mm at the condition of Re= 800 in both V-type and P-type components. The same trend occurs in Fig. 8 (a) and (b) when Re was 4800. The values of d_{VAM} are much smaller and almost all the values of d_{VAM} are below 0.5 mm. Moreover, d_{VAM} tends to be stable after the position to be x=3 mm.

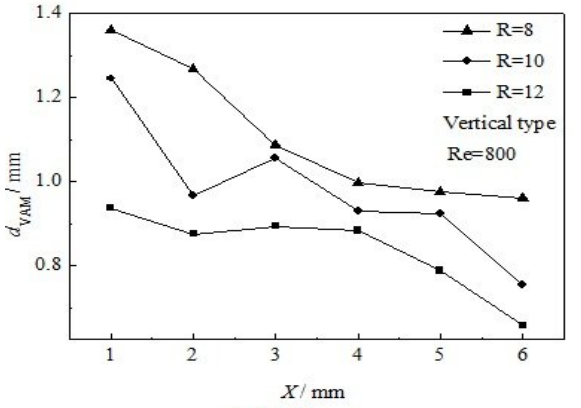

(a) V-type

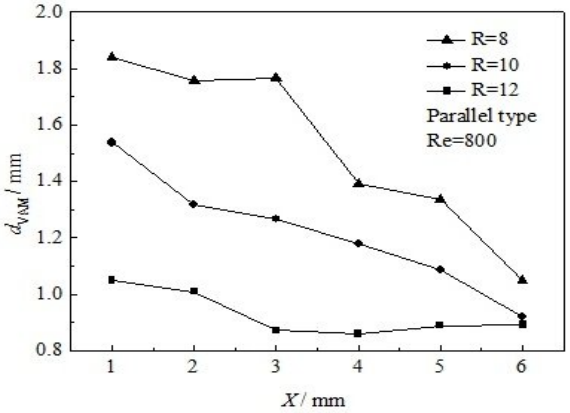

(b) P-type charging component

(a) V-type and (b) P-type charging component

Fig. 7: Effect of charging position on d_{VAM} at Re=800.

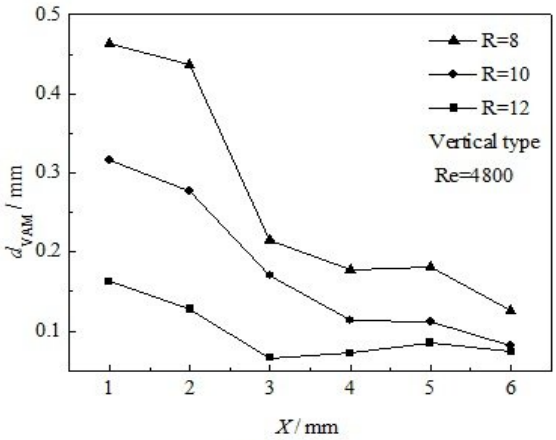

(a) V-type

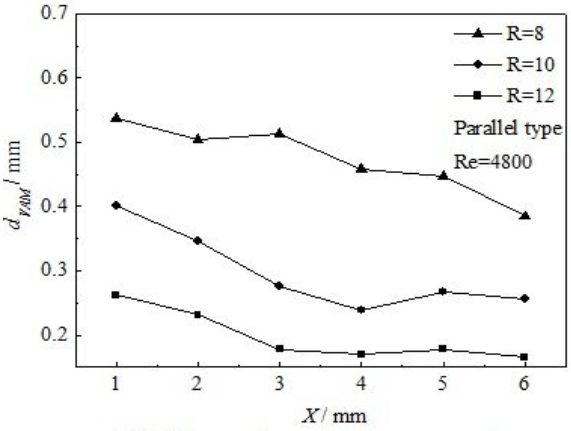

(b) P-type charging component

(a) V-type and (b) P-type charging component

Fig. 8: Effect of charging position on d_{VAM} at Re=4800.

Correlation of d_{VAM} in HTR with different charging components

A correlation taking effects of Reynolds number, volumetric flow ratio of water to oil, and charging position into consideration was proposed for the calculation of SMD as shown in Eq.(14), where d_i was inner diameter of HTR and L was the length of charging section.

$$\frac{d_{VAM}}{d_i} = \begin{cases} 12848\,\mathrm{Re}^{-1.12} R^{-1.53} \left(\frac{x}{L}\right)^{-0.27} & (for\ V-type) \\ 7220\,\mathrm{Re}^{-0.96} R^{-1.70} \left(\frac{x}{L}\right)^{-0.33} & (for\ P-type) \end{cases} \quad (14)$$

From the correlation, we could find the dependence of d_{VAM} on *R*e in the HTR with V-type charging component was higher than that with P-type one. In the HTR with P-type charging component, the dependence of d_{VAM} on both *R* and dimensionless position (*x*/*L*) was higher that with V-type charging component. As shown in Fig. 9, the maximum deviation of the correlation from the experimental data was within ±20%. The above correlation could be beneficial for the design of HTR since keeping similar values of the effective interfacial area was very important for the scale-up design.

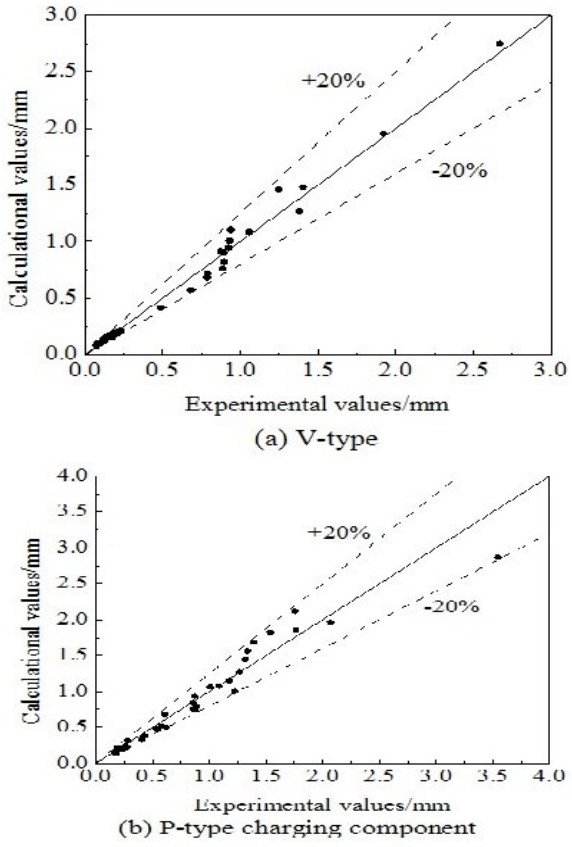

Fig. 9: Experimental vs. calculation values

Conclusions/ Acknowledgements

The size of the dispersed phase in a novel HTR was studied by using a chemical method. Compared with the straight tube, SMD in the HTR decreased by 47.2~75% and 38.1~48.5% in low and high *R*e region, respectively. The smallest SMD was below 0.1 mm. The HTR with a V-type charging component showed better dispersing performance than that with a P-type charging component. Larger *R*e resulted in a smaller SMD. For the same values of *R*e, the SMD in the HTR decreased with the increase of volumetric flowrate ratio from 8 to 12. When the charging position was varied from *x*=1 to 6 mm, the SMD decreased and almost became stable after the position of *x*=3 mm at the condition of *R*e=4800. Moreover, a dimensionless correlation was proposed for calculating the SMD in the HTR, and the deviation between the experimental and calculated data was within ±20%.

This work was supported by the National Natural Science Foundation of China (Nos. 21406008, U1462127, and 21436001).

Nomenclature

a	Interfacial area per unit volume, m^2/m^3
C_A	Molar concentration of A, mol/L
C_B	Molar concentration of B in continuous phase, mol/L
C_C	Molar concentration of acetic acid in continuous phase, mol/L
d_{VAM}	Sauter mean diameter of dispersed phase, mm
d_i	Diameter of the inner tube, mm
K_a	Apparent heterogeneous reaction rate constant, $m^4/(mol\ s)$
K'	$K' = K_a C_A$ =1.384×10^{-3} m/s in our
L	Length of the charging section, mm
N	Droplet number of dispersed phase
Q_A	Volumetric flowrate of continuous phase, L/s
Q_B	Volumetric flowrate of dispersed phase, L/s
R	Volumetric flowrate ratio of continuous phase to dispersed phase, [-]
V_A	Volume of continuous phase in reactor, m^3
V_B	Volume of dispersed phase in reactor, m^3
V_R	Effective volume of helical tube reactor, m^3
x	Charging position along the *x*-coordinate (as shown in Fig. 2), mm
τ	Mean residence time in helical tube reactor, s

References

1. S. Vashisth, V. Ku mar and K. D. P. Nigam, A review on the potential applications of curved geometries in process industry, *Ind. Eng. Chem. Res*., **47**, 3291 (2008).
2. M. Mridha, K. D. P. Nigam, Numerical study of turbulent forced convection in coiled flow inverter, *Chem. Eng. Process*., **47**, 893 (2008).

3. S. Vashisth, K. D. P. Nigam, Prediction of flow profiles and interfacial phenomena for two-phase flow in coiled tubes, *Chem. Eng. Process.*, **48**, 452 (2009).
4. S. Chingulpitak, S. Wongwises, Two-phase flow model of refrigerants flowing through helically coiled capillary tubes, *Appl. Therm. Eng*., **30**, 1927 (2010).
5. A. P. Sasmito, J. C. Kurnia and A. S. Mujumdar, Numerical evaluation of transport phenomena in a T-junction microreactor with coils of different configurations, *Ind. Eng. Chem. Res*., **51**, 1970 (2012).
6. J. C. Kurnia, A. P. Sasmito and A. S. Mujumda, Laminar convective heat transfer for in-plane spiral coils of non-circular cross-sections ducts: A computational fluid dynamics study, *Therm. Sci*., **16** (1), 109 (2012).
7. M. M. Mandal, K. D. P. Nigam, Experimental study on pressure drop and heat transfer of turbulent flow in tube in tube helical heat exchanger, *Ind. Eng. Chem*. *Res*., **48**, 9318 (2009).
8. M. M. Mandal, C. Serra, Y. Hoarau and K. D. P. Nigam, Numerical modeling of polystyrene synthesis in coiled flow inverter, *Microfluid. Nanofluid*., **10**, 415 (2011).
9. J. Singh, V. Verma and K. D. P. Nigam, Flow characteristics of power-law fluids in coiled flow inverter, *Ind. Eng. Chem. Res*., **52**, 207 (2013).
10. M. Torab-Mostaedi, A. Ghaemi and M. Asadollahzadeh, Flooding and drop size in a pulsed disc and doughnut extraction column, *Chem. Eng. Res. Des*., **89**, 2742 (2011).
11. C. V. Lakshmi, K. Viswanath, S. Venkateshwar and B. Satyavathi, Mixing characteristics of the oil-methanol system in the production of biodiesel using edible and non-edible oils, *Fuel. Process. Technol*., **92**, 1411 (2011).
12. K. Yoneda, A. Yasuo and T. Okawa, Flow structure and bubble characteristics of steam-water two-phase flow in columns of different diameter, *Int. J. Multiphase. Flow*., **217**, 267 (2002a).
13. K. Yoneda, A. Yasuo and T. Okawa, Bubble characteristics of steam-water two-phase flow in a large-diameter pipe, *Exp. Therm. Fluid. Sci*., **26**, 669 (2002b).
14. S. H. Park, H. J. Kim, H. K. Suh and C. S. Lee, A study on the fuel injection and atomization characteristics, *Int. J. Heat. Fluid*., **30**, 108 (2009).
15. P. Angeli, G. F. Hewitt, Drop size distributions in horizontal oil-water dispersed flows, *Chem. Eng. Sci*., **55**, 3133 (2000).
16. K. R. Westerterp, L. L. Van Dierendonck and J. A. De Kraa, Interfacial areas in agitated gas-liquid contactors, *Chem. Eng. Sci*., **18**, 157 (1963).
17. J. M. Zaldicar, E. Molga, M. A. Alos, H. Hernandez and K. R. Westerterp, Aromatic nitrations by mixed acid: Fast liquid-liquid reaction regime, *Chem. Eng. Process*., **35**, 91 (1996).
18. B. A. A. Van Woezik, K. R. Westerterp, Measurement of interfacial areas with the chemical method for a system with alternating dispersed phases. *Chem. Eng. Process*., **39**, 299 (2000).
19. R. Z. Liang, J. W. Li, The optimum pilot volume in heterogeneous nitration reactor, *Sci. Tec. Chem. Ind*., **8**, 5 (2000). (in Chinese).
20. P. A. Quadros, C. M. S. G. Baptista, Effective interfacial area in agitated liquid-liquid continuous reactors, *Chem. Eng. Sci*., **58**, 3935 (2003).